Stimulated nutation echo: application to the driven decoherence study

2003 J. Phys.: Condens. Matter 15 4215

(http://iopscience.iop.org/0953-8984/15/24/315)

INSTITUTE OF PHYSICS PUBLISHING JOURNAL OF PHYSICS: CONDENSED MATTER

J. Phys.: Condens. Matter **15** (2003) 4215–4228 PII: S0953-8984(03)59269-4

Stimulated nutation echo: application to the driven decoherence study

G Bimbo[1], R Boscaino[1,4], M Cannas[1], F M Gelardi[1] and R N Shakhmuratov[2,3]

[1] Istituto Nazionale per la Fisica della Materia and Department of Physical and Astronomical Sciences, University of Palermo, Via Archirafi 36, I 90123 Palermo, Italy
[2] Kazan Physical Technical Institute of Russian Academy of Sciences, 10/7 Sibirski trakt, Kazan, 420029, Russia
[3] Instituut voor Kern-en Stralingsfysica, Katholieke Universiteit Leuven, Celestijnenlaan 200D, B-3001 Leuven, Belgium

E-mail: boscaino@fisica.unipa.it

Received 5 February 2003
Published 6 June 2003
Online at stacks.iop.org/JPhysCM/15/4215

Abstract

We study experimentally the dynamical and decay properties of the stimulated nutation echo (SNE) in a two-level spin system, the signal of which allows the observation timescale of the driven coherence relaxation to be extended. This signal appears in the transient response of the system to the second pulse at time τ_1 from its start and coinciding with the duration of the first pulse. The information about the first pulse duration is imprinted into the population difference of the inhomogeneously broadened ensemble of the two-level absorbers. The decay of the SNE signal has two contributions. One originates from the population decay during the time τ between the two pulses. Another is caused by the coherence loss during the excitation by the first pulse and the reading time of the second pulse. Experimental results on the decay properties induced by these mechanisms are presented for the first time. We investigate the dependence of these decay rates on the pulse intensity and we examine its relationship with the anomalous (non-Bloch) decay of other coherent transients in solids.

1. Introduction

Coherence decay is a crucial point in atom–field interaction. It determines the accuracy limit of the atom state manipulation and preparation in a particular coherent or pure state by the sequence of two or more coherent pulses of resonant radiation. Decoherence takes place both between pulses when atom evolves freely (free decoherence) and during the excitation (driven

[4] Author to whom any correspondence should be addressed.

decoherence). In solids, an additional (reversible) contribution to dephasing originates from the inhomogeneous spread of the resonance frequencies. While free irreversible decoherence can be studied quite well by two-pulse echo on a long timescale, the measurement of the driven decoherence is rather complicated. For example, consider an ensemble of two-level atoms with an inhomogeneously broadened transition. One can find the actual T_2 (homogeneous dephasing time) during the excitation by measuring the free induction decay (FID) rate. In fact, even if FID is the signal emitted by the system after abruptly switching off the radiation pulse, it images the spectral properties of the stationary state reached during the pulse. In the high power limit, FID is expected to decay at the rate $\sim\chi\sqrt{T_1/T_2}$, where T_1 is the relaxation time of the population difference and χ is the driving field Rabi frequency. So, one can infer the driven T_2 from FID measurements if T_1 and χ are known. In solids at low temperature, narrow lines (for example, the R_1-line in ruby and the $^3H_4$–$^1D_2$ transition in Pr^{3+}:LaF_3) have appreciably long decay times ($\approx$ms) for the excited state, limited mainly by spontaneous emission. The coherence decay is mostly caused by magnetic dipole interaction and hence the irreversible dephasing time T_2 (scaled in tens of microseconds) is much shorter than T_1. Anomalous behaviour of the driven decoherence rate was found in FID [1–6] and hole burning [7] experiments: the driven T_2 deduced from FID or from saturated hole width was found to be much longer than the free decoherence time and to increase on increasing the driving field amplitude up to the vacuum limit $\sim 2T_1$.

The results for the optical domain [1, 3, 6, 7] are similar to those obtained for electron spin resonance (ESR) systems [2, 4, 5] and one can assume that both systems (optical and spin two-level systems) are nearly identical in this respect. Both are affected by magnetic dipole interactions and both have high inhomogeneous broadening. There are some advantages in considering ESR systems when studying experimentally the decay of coherent regimes. As T_1 and T_2 are longer than in optical systems, simpler electronics is required for exploring the decay timescale. Moreover, tunable sources of microwave radiation with very narrow spectral widths (<1 Hz) are available. So, in these systems, the direct measurement of the driven T_2 was possible also using another coherent regime, the transient nutations (TN). This is the transient regime of system when the power pulse is switched on and the emitted signal is expected to decay as $V_{TN} \propto J_0(\chi t)\exp(-t/2T_2)$. Our TN experiments revealed that the driven dephasing time T_2, measured during the TN regime, is much shorter than the free decoherence time and decreases on increasing the driving field amplitude [8, 9].

The evident conflict between the power dependence of the driven decoherence time T_2, measured by FID and by TN experiments, was ascribed to the dipolar reservoir squeezing [9, 10] resulting in two different driven decoherences, i.e. in-phase dephasing T_{2u} and out-of-phase dephasing T_{2v}. In this regard, it has been shown that field-induced modifications of the dipolar interaction produce essentially the same effect as the driving field noise [10–12]. The driven dipolar reservoir contributes also to the T_1 relaxation, which becomes dependent on the resonant detuning. The interplay between driven T_{2u}, T_{2v} and T_1 relaxation times explains FID and TN behaviour apparently contradicting with each other and with the predictions of the conventional Bloch equations.

Besides our theory, another approach was proposed in [13–15] explaining the anomalous power dependence of the decay rates of coherent transients by different dependences of T_{2u} and T_{2v} on the driving field amplitude and constant T_1. The in-phase decoherence rate, T_{2u}^{-1}, reduces to the vacuum limit, $(2T_1)^{-1}$, and the out-of-phase one, T_{2v}^{-1}, rises linearly with the driving field amplitude. T_{2u}, appearing in the expression for the hole width, determines the FID rate, whereas T_{2v} is just the time constant in the exponential factor of the TN decay. Theories, presented in [9–15], differ qualitatively from theoretical treatments [16–24], which have been proposed to explain only the anomalous FID rate (the list is not exhaustive).

It should be remembered that the oscillating and fast decaying part of the TN, described by the Bessel function $J_0(\chi t)$, originates from the destructive interference of the Rabi oscillations, which are different for resonant absorbers having different resonant frequencies. This reversible contribution to the TN decay limits the measurement accuracy of the driven T_2, but it is intrinsic to solid systems. Therefore, for studying the driven decoherence it is important to look for another transient regime, whose decay is unaffected by the reversible contribution caused by the inhomogeneous broadening. The appropriate candidates for this purpose are the driven transient echo phenomena.

In this paper we use the stimulated nutation echo (SNE) [25–31] to extend the timescale of the driven T_{2v}-dephasing measurement. To our knowledge, this is the first application of SNE to the study of driven decoherence. Until now, it has been used only to study T_1 and spectral diffusion (SD) processes [27–31].

SNE takes place in the following conditions. When a system of two-level centres (atoms or spins) is resonantly driven by a sequence of two pulses, lasting τ_1 and τ_2 and separated by the interpulse distance τ, the response of the system to the second pulse ($t > \tau_1 + \tau$) includes both an initial Rabi-oscillating component and an oscillatory echo, centred at $t = 2\tau_1 + \tau$, namely at a time distance τ_1 from the onset of the second pulse. This echo is an example of forced echo (see [32] for a recent review), in the sense that it occurs during the second refocusing pulse and is emitted by a strongly driven rather than by a freely evolving system.

The nutation echo effect originates from the fact that first pulse burns a sequence of holes in the inhomogeneous spectrum. For $T_2 \sim \tau_1 \ll T_1$, the hole burning process is strongly affected by the decoherence but not by the T_1 relaxation. If the distance τ between the two pulses is shorter than T_1, at the onset of the second pulse the system keeps a memory of its time evolution during the first (preparative) pulse. As a consequence, it exhibits a sort of revival of Rabi nutations during the second pulse, which occurs when the usual TN signal has nearly vanished, so that two coherent regimes can be isolated from each other. Even if the nutation echo signal looks like the revival of initially strong but fast decaying TN oscillations induced by the second pulse, actually it originates from the spectral pattern established during the first pulse.

It is worth noting that the phase coherence and the phase shift between the two exciting pulses are not relevant in the echo effect considered here. In this respect, it is different from the spin and optical rotary echo [33, 34], from nutation time-reversal experiments [35] and from coherent echoes excited by field gradient sequences in NMR imaging [36]. Moreover, the nutation echo is investigated here in ESR systems in such conditions that it originates only from the spectral pattern of the population difference stored in the inhomogeneous spectrum at the end of the first pulse. Following [30, 31], we refer to it as SNE, in analogy to the three-pulse-stimulated echo that is produced from a hole pattern burnt into an inhomogeneous line. At variance with previous observations of SNE in ESR systems, obtained either in spin systems generated by pulsed light irradiation [27], or by indirect optical detection [28], or by applying Zeeman field pulses [29], in our experiments the SNE is directly excited by pulses of resonant radiation. This configuration yields a high value of the signal-to-noise ratio.

We report experimental results on the decay properties of the SNE signal. The SNE intensity decays both when the interpulse distance τ is increased and on lengthening the first pulse duration τ_1. The former decay is caused by the thermalization of the population difference pattern. According to the conventional Bloch equations, this decay should proceed at the rate T_1^{-1}. However, the results reported here show that this decay is governed by the SD process, which is sensitive to the spectral pattern established by the first pulse. On the other hand, the decay of the SNE on increasing the duration τ_1 of the first (exciting) pulse is due to the driven coherence loss mechanisms. We find that also this decay rate depends on the driving field intensity and this aspect is our major point of interest.

The paper is organized as follows. In section 2 we briefly outline the theory of the SNE by Szabo and Shakhmuratov [30, 31] for calculating the intensity and the shape of the SNE and its decay properties, tailoring it to the specific system considered here and hypothesizing the phenomenological Bloch times T_1 and T_2 (T_{2u}, T_{2v}). In section 3 we report the experimental results obtained in our ESR system. In section 4 we compare our results with the solutions of the Bloch equations and with the anomalous decay of the TN experimentally observed in the same system.

2. Theory

In this section we give a brief and simplified sketch of the theory of the SNE presented in [30, 31] and we take into account the relaxation phenomena, to make clear the discussion of the results and to address the question which decoherence time, T_{2u} or T_{2v}, determines the SNE decay.

We consider an inhomogeneous system of two-level particles whose frequencies ω are spread around the mean frequency ω_0 according to a symmetric distribution $f(\omega - \omega_0)$. The resonance line is the convolution of the inhomogeneous distribution with much narrower homogeneous lines (hereafter referred to as spin packets). The system is excited by a sequence of two pulses of resonant radiation tuned at the line centre ω_0, lasting τ_1 and τ_2, and separated by τ.

The time evolution of the generic spin packet, characterized by its detuning $\Delta = \omega - \omega_0$ from the line centre and from the radiation, is described by the Bloch-vector components $u(\Delta, t)$, $v(\Delta, t)$ and $w(\Delta, t)$, which are combinations of the elements of the particle density matrix ρ: $u + \mathrm{i}v = 2\rho_{12}\exp(-\mathrm{i}\omega_0 t)$, $w = \rho_{22} - \rho_{11}$. The transient response of the whole system is the superposition of the responses of the individual packets weighted by the distribution $f(\Delta)$. For the resonant excitation considered here, the only non-vanishing coherence of the system is

$$\langle v(t)\rangle = V(t) = \int_{-\infty}^{+\infty} v(\Delta, t) f(\Delta)\,\mathrm{d}\Delta \tag{1}$$

and we limit ourselves to calculating $v(\Delta, t)$.

The time evolution of the generic packet is governed by the Bloch equations:

$$\dot{u} + \Delta v + u/T_{2u} = 0, \tag{2}$$

$$\dot{v} - \Delta u - \chi w + v/T_{2v} = 0, \tag{3}$$

$$\dot{w} + \chi v + (w - w_0)/T_1 = 0, \tag{4}$$

where w_0 is the equilibrium population difference. T_1, T_{2u} and T_{2v} are the decay times of the population difference w and of the coherences u and v, with $T_1 \gg T_{2u}, T_{2v}$. The Rabi frequency χ is defined by the transition matrix element and the amplitude of the driving field. For $T_{2u} = T_{2v} = T_2$, equations (2)–(4) coincide with the conventional Bloch equations, whose transient solutions were derived by Torrey [37]. We consider here modified Torrey solutions to cover the case $T_{2u} \neq T_{2v}$. The solution simplifies if we assume the strong field limit ($\chi T_2 \gg 1$) and that the first pulse duration τ_1 is much shorter than T_1, so that only T_{2u} and T_{2v} affect the time evolution of the system during the pulses. Both conditions are well satisfied in our experimental situation. During the first (preparative) pulse the generic packet precesses at the frequency $\beta = \sqrt{\Delta^2 + \chi^2}$ around its effective field. At the end of the pulse, its population difference is given by:

$$\frac{w(\Delta, \tau_1)}{w_0} = \alpha_2 \exp\left(-\alpha_1 \frac{\tau_1}{T_{2u}}\right) + \alpha_1 \exp\left(-\frac{\tau_1}{2T_{2v}} - \frac{\alpha_2 \tau_1}{2T_{2u}}\right)\cos(\beta\tau_1) \tag{5}$$

where $\alpha_1 = (\chi/\beta)^2$ and $\alpha_2 = (\Delta/\beta)^2$.

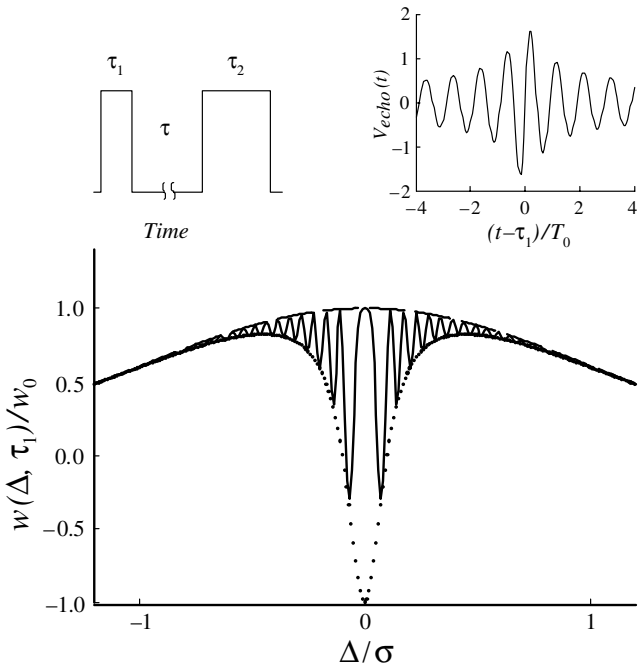

Figure 1. Spectral pattern of the population difference at the end of the first pulse. The dashed curve plots the Gaussian inhomogeneous line with standard deviation σ. The full curve plots the population difference, as calculated from equation (4), with $\chi/\sigma = 0.2$, $\tau_1/T_0 = 2$, $T_2/T_0 = 2000$. The dotted curve is the envelope of the hole burnt within the inhomogeneous curve. The inset on the right side shows the corresponding SNE signal: time t is measured from the beginning of the second pulse and is given in units of the Rabi period T_0. The inset on the left side sketches the pulse sequence.

The spectral pattern described by equation (5) is the ultimate origin of the echo effect we are concerned with. A typical result is given in figure 1, as obtained from equation (5), assuming a Gaussian inhomogeneous line shape with standard deviation σ. As shown, $w(\Delta, \tau_1)$ is strongly modulated within a spectral region of width χ around the excitation point (the line centre in our case). Obviously, the particular pattern depends both on χ and on τ_1: on increasing χ this region broadens and on increasing τ_1 the peaks become closer and closer.

After the first pulse ($t > \tau_1$), the spins evolve freely during the interpulse distance τ. We assume that τ is long enough to ensure the complete decay of the coherences $u(\Delta, \tau_1)$ and $v(\Delta, \tau_1)$ induced by the first pulse. As shown in [31], their contribution to the SNE signal decays as $\propto \exp(-\chi\tau)$. So, provided that τ is much longer than the Rabi period $T_0 = 2\pi/\chi$, at $t = \tau + \tau_1$ (onset of the second pulse) the memory of the nutational regime excited by the first pulse is stored only in the spectral distribution $w(\Delta, \tau_1)$, damped by the T_1 relaxation:

$$\begin{aligned} &w(\Delta, \tau_1 + \tau) = [w(\Delta, \tau_1) - w_0]\exp(-\tau/T_1) + w_0, \\ &u(\Delta, \tau_1 + \tau) = 0;\ v(\Delta, \tau_1 + \tau) = 0. \end{aligned} \tag{6}$$

These equations represent the initial conditions of the system at the onset of the second pulse.

During the second pulse, the v-component of the induced coherence is

$$v(\Delta, t) = \left(\frac{\chi}{\beta}\sin\beta t\right)\exp\left(-\frac{t}{2T_{2v}} - \alpha_2\frac{t}{2T_{2u}}\right)w(\Delta, \tau_1 + \tau), \tag{7}$$

as obtained by solving equations (2)–(4) again with the initial conditions in equation (6). Here t is the time counted from the beginning of the second pulse. By substituting equations (5) and (6), we get:

$$\frac{v(\Delta,t)}{w_0} = \frac{\chi}{\beta}\sin(\beta t)\exp\left(-\frac{t}{2T_{2v}}-\frac{\alpha_2 t}{2T_{2u}}\right)\left\{1-\exp\left(-\frac{\tau}{T_1}\right)+\alpha_2\exp\left(-\frac{\tau}{T_1}-\frac{\alpha_1\tau_1}{T_{2u}}\right)\right\}$$
$$+\frac{1}{2}\left(\frac{\chi}{\beta}\right)^3\exp\left[-\frac{\tau}{T_1}-\left(\frac{1}{2T_{2v}}+\frac{\alpha_2}{2T_{2u}}\right)(\tau_1+t)\right]$$
$$\times[\sin(\beta(t-\tau_1))+\sin(\beta(t+\tau_1))]. \tag{8}$$

The time response of the whole system is finally obtained by inserting equation (8) into equation (1) to get $V(t)$. We assume that the width of the inhomogeneous distribution is much higher than χ, so that we can consider the integration in equation (1) as the integration with the flat function $f(\Delta) = f(0)$. Hereafter, to simplify the calculation we admit $\alpha_1 = 1$ and $\alpha_2 = 0$.

In equation (8), the first term represents the TN induced by the second pulse, originating from the almost nonperturbed part of the thermal population difference and can be considered as a supplementary signal, in which we are not interested. Here we are interested in the term containing $\sin(\beta(t-\tau_1))$, which represents the SNE signal $V_{echo}(t)$, centred at $t = \tau_1$. Then

$$\frac{V_{echo}(t)}{w_0} = \frac{1}{2}f(0)\exp\left(-\frac{\tau_1+t}{2T_{2v}}-\frac{\tau}{T_1}\right)\int_{-\infty}^{+\infty}\left(\frac{\chi}{\beta}\right)^3\sin(\beta(t-\tau_1))\,\mathrm{d}\Delta. \tag{9}$$

A typical result of the SNE signal, as calculated using equation (9), is reported in the inset of figure 1. The signal consists of an oscillatory pattern with many spikes of alternating sign. The peak values are distributed inside a symmetric bell-shaped envelope centred at $t = \tau_1$. According to the analytical study carried out in [30, 31], the spikes occur at $t = \tau_1 \pm t_i$, where the sequence t_i is given in units of the Rabi period T_0 as $t_i/T_0 = 0.17, 0.65, 1.24, 1.74, 2.24$, etc. The amplitudes of the spikes decrease as t_i increases. V_{echo} is exactly zero at $t = \tau_1$.

The SNE is well pronounced if the first pulse area $\theta = \chi\tau_1$ is at least several π; otherwise it is impossible to isolate the echo signal from the TN excited by the second pulse, given by the first term in equation (8). Varying the time parameters of the exciting sequence, τ_1 and τ, the amplitudes V_m of the peaks nearest to the centre ($t \approx \tau_1$) are expected to be damped as:

$$V_m \propto \exp\left(-\frac{\tau_1}{T_{2v}}-\frac{\tau}{T_1}\right). \tag{10}$$

SNE is expected to decay on increasing the interpulse distance τ at a rate fixed by the spin relaxation time T_1. On the other hand, the SNE echo is also expected to decay as a function of τ_1 as a single exponential at the rate $1/T_{2v}$. In this regard we remark that this expectation is not conditioned by the approximation used for α_1 and α_2. In fact, by numerically integrating equation (8) using the Δ-dependent expression of α_1 and α_2, we verified that the only effect of the approximation is to overestimate the decay rate (by nearly 10%), in the sense that the actual rate is $1.13/T_2$ rather than $1/T_2$ if the relation $T_{2u} = T_{2v} = T_2$ is taken. What is important for our present concern is that the single exponential nature of the decay and the χ-independence of the rate are properties of the exact solution of the Bloch equations. This is the reason why an interest in this coherent regime is so relevant. In fact, the decay of the SNE as a function of τ_1 should manifest the processes of coherence loss in the strongly driven system. As mentioned in the previous section, in these regimes the decay properties deviate strongly from those predicted by the Bloch equations. This has been already observed in connection with the TN regime [8, 9] and a similar effect is expected to occur for the SNE.

3. Experiments

For the experimental investigation of the SNE in magnetic resonance systems we used the two-photon (TP) excitation, second-harmonic (SH) detection method, already successfully employed for several transient regimes [2, 4, 8]. In our experimental apparatus, the spin system, tuned to the frequency ω_0 ($\omega_0/2\pi = 5.95$ GHz) by the external static magnetic field B_0, is excited by an intense microwave radiation at frequency $\omega = \omega_0/2$, which couples the spin states by TP transitions. The TP-induced coherences manifest themselves in the build-up of a transverse magnetization, $M_\perp(2\omega)$, oscillating at the SH of the driving field. The response of the spin system is monitored by revealing the radiation emitted by the spin system at frequency 2ω. Under pulse excitation conditions, the amplitude $M_\perp$ of $M_\perp(2\omega)$ varies in time, reproducing the coherent transient regimes of the spin system. At the exact TP tuning, $\omega = \omega_0/2$, $M_\perp$ is proportional to the average coherence $V(t)$ (equation (1)) and is the same as for the usual single-quantum excitation, provided that the appropriate TP-induced Rabi frequency χ is used [38, 39]. In our experimental set-up $\chi/2\pi$ can be varied from 10 to 250 kHz. We refer to our previous papers [2, 4, 8] for the detailed description of this procedure and of the related experimental apparatus.

The experiments described below were carried out at $T = 4.2$ K, using a sample of glassy SiO_2 containing a concentration $c \sim 2.4 \times 10^{17}$ spin cm^{-3} of E' centres, preliminarily generated by exposure to gamma rays [40]. E' centres have $S = 1/2$ and are particularly suitable for this kind of experiment due to their relatively long relaxation times. In our work conditions, we measured $T_1 = 1.2$ s (by the saturation recovery method) and $T_2 = 75$ μs (by the spin echo method, which gives the free decoherence time). In the glassy matrix of SiO_2, E' centres exhibit a powder-like line shape. For the purposes of the experiments described below, the central part of their resonance line is well approximated by a Gaussian shape with $\sigma/2\pi \sim 1$ MHz. Due to the high value of σT_2 ($\approx 5 \times 10^2$), the high-inhomogeneity approximation, used in deriving equation (9), is well fulfilled in our system.

The spin system, tuned at resonance, is excited by a sequence of two pulses, lasting τ_1 and τ_2 respectively, separated by a distance τ, both with the same power level. The repetition frequency is kept low enough (typically 0.5 Hz) to ensure adequate thermal relaxation of the spin system between successive sequences. The microwave signal emitted by the spin system and output by the cavity has a time-dependent amplitude $M_\perp(t)$, which we detect by a phase insensitive superheterodyne receiver to get $|M_\perp(t)|$. To improve the signal-to-noise ratio, $|M_\perp(t)|$ is averaged over typically 16 sequences.

During the first pulse, the system undergoes damped Rabi oscillations, which we use for the accurate measure of χ. A typical response to the second pulse is shown in figure 2, as detected for $\chi/2\pi = 200$ kHz, $\tau_1 = 30$ μs ($\tau_1 \approx 6T_0$) and $\tau = 400$ μs ($\tau \gg T_0, T_2$). At the onset of the second pulse, the system undergoes fast-damping Rabi oscillations, followed by the SNE regime. The SNE signal consists of a bell-enveloped series of peaks, centred at $t_e = 30$ μs ($t_e = \tau_1$) after the onset of the second pulse, in agreement with theoretical predictions.

In order to explore the ranges of low values of χ and of long values of τ_1 and τ, where the SNE signal is close to the noise level, we often used a sort of homodyne detection. The microwave signal output by the cavity is first superimposed on a reference signal with the same frequency, whose amplitude and phase are adjusted to optimize the visibility of SNE oscillations. The sum signal is then revealed by a conventional superheterodyne detector, yielding $S^2(t) = M_\perp^2 + R^2 + 2M_\perp R$, where R is the amplitude of the reference signal. The result is shown in the inset of figure 2. Usually, $R^2 \gg M_\perp^2$, so that $S^2 \approx R^2 + 2M_\perp R$ consists of a dc offset and a time-dependent part reproducing the time evolution of $M_\perp(t)$, coherently

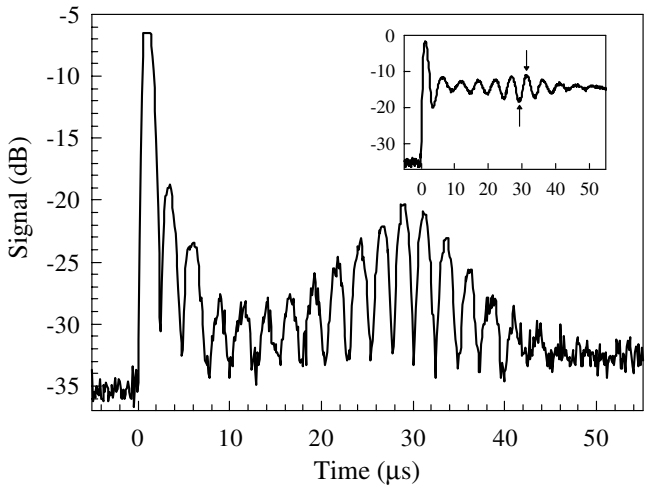

Figure 2. Typical SNE signal, as detected after a preparative pulse with $\chi/2\pi = 200$ kHz and lasting $\tau_1 = 30$ μs. Time t is measured from the onset of the second pulse, 400 μs after the first one. The same signal is shown in the inset, as detected using the superposition to a reference signal and described in the text. The arrows point the maximum and the minimum used for evaluating the SNE amplitude V_m, as described in the text.

amplified by the reference signal. To estimate the SNE amplitude V_m, we measured the maximum and the minimum signals nearest to the echo centre (indicated by arrows in the inset of figure 2): S^2_{max} $(=M^2_\perp + R^2 + 2|M_\perp|R)$ and S^2_{min} $(=M^2_\perp + R^2 - 2|M_\perp|R)$ to get $V_m \propto |M_\perp|$ as $[(S^2_{max} - S^2_{min})/4R]^{1/2}$. To use the maximum and the minimum nearest to the echo centre for measuring the echo amplitude V_m is convenient as they offer the highest amplitude. Whenever possible, we verified that the decay properties considered below are essentially the same for any other maximum or minimum, at least in the investigated range of T_0 and of τ_1.

The detailed timing of the SNE signal is shown in figure 3 where we report the expanded view of a typical curve of the SNE signal, taken with a Rabi frequency $\chi/2\pi = 100$ kHz and $\tau_1 = 55$ μs. In the figure the time origin is placed at 55 μs after the onset of the second pulse (namely, at the expected centre of the SNE signal) and we observe maxima and minima, symmetrically located around the origin, at times t_i where $t_i/T_0 = 0.25$, 0.72, 1.23, 1.74 and 2.27 (± 0.02, typically) in units of the Rabi period T_0. The symmetrical location around the echo centre was observed for several values of T_0 and of τ_1, within the experimental uncertainties, for those maxima and minima that are well separated from the Rabi oscillations excited by the second pulse. The agreement with the theoretical values, 0.17, 0.65, 1.24, 1.74 and 2.24, is fair, except for the first two extrema. This aspect will be commented on in the conclusion. Here we note that, as the explored range of T_0 is from 5 to 50 μs, the measured distance between the maximum and the minimum nearest to the echo centre varies from 2.5 to 25 μs, well above the response time of our detection system.

We investigated the decay of the SNE signal both as a function of the interpulse distance τ and of the first pulse duration τ_1, paying particular attention to the power dependence of both decay kinetics.

In a first set of experiments the duration τ_1 of the preparative pulse and the power level were kept fixed and the echo amplitude V_m was measured as a function of τ. The measurements were repeated for various values of $\chi/2\pi$, ranging from 75 to 208 kHz. The results are reported in figure 4. As shown, the decay curves are not single exponentials and occur in a timescale of

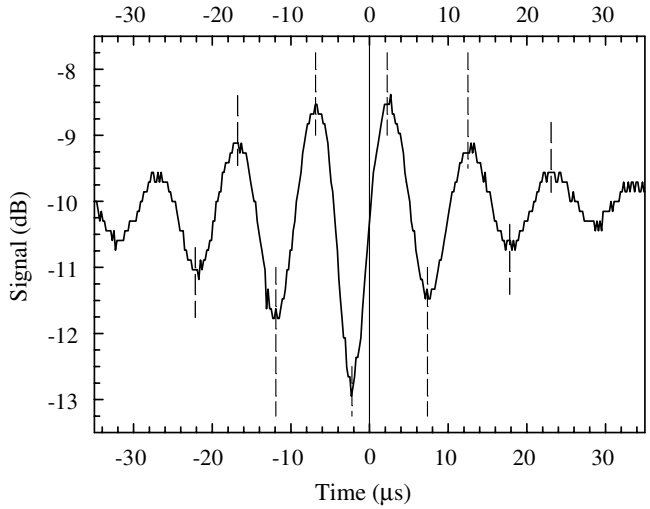

Figure 3. Timing of the SNE signal, taken with $\chi/2\pi = 100$ kHz, $\tau_1 = 55$ μs, $\tau = 40$ μs. The time origin is placed at 55 μs after the onset of the second pulse and coincides with the centre of the SNE signal. Dashed lines indicate the maxima and minima, occurring at the values t_i listed in the text.

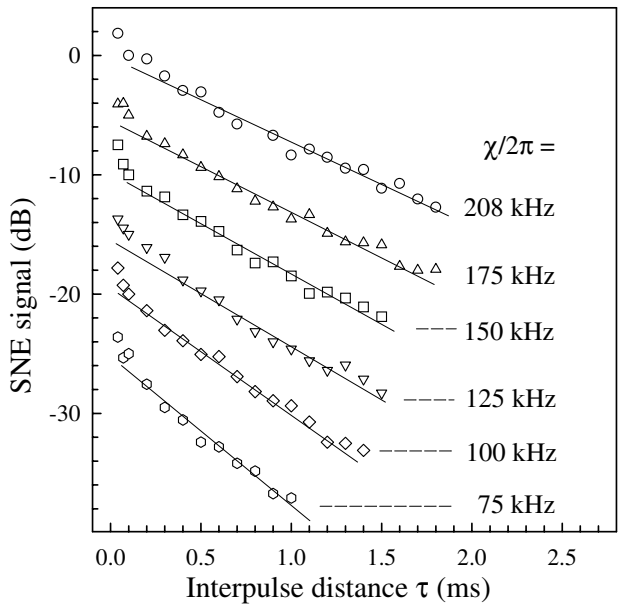

Figure 4. Decay of the SNE signal on varying the interpulse distance τ, at various values (indicated in the figure) of the Rabi frequency χ. Symbols are experimental values of SNE intensity, measured as described in the text. Lines are only guides for eyes. The curves are shifted vertically to optimize the visibility.

a few milliseconds, much shorter than the relaxation time T_1 ($\sim$1.2 s). It is worth noting that the time shape of the SNE signal does not change on varying τ, so that each curve in figure 4 reproduces the decrease of SNE at any time. On varying χ, the decay properties change, in

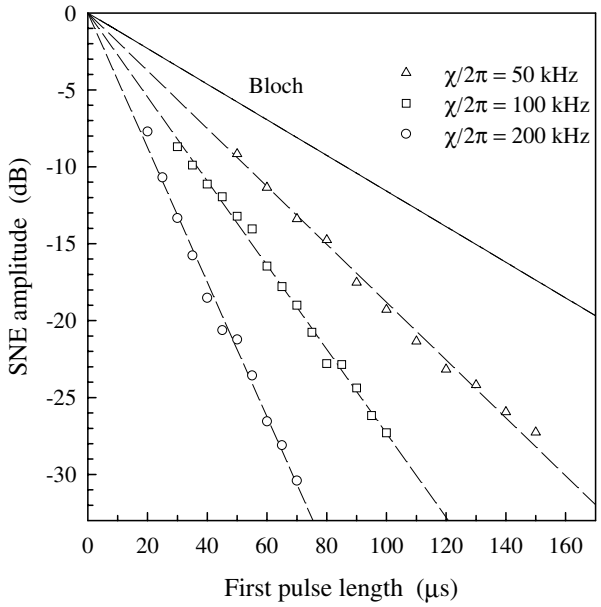

Figure 5. Decay of the SNE amplitude V_m on varying the duration τ_1 of the first (exciting) pulse, for three values of the Rabi frequency, indicated in the figure. The interpulse distance is $\tau = 150\ \mu$s. The dashed lines are the exponential laws that best fit the experimental points and are used to measure Γ_E. The full line represents the decay curve expected on the basis of the Bloch equation.

the sense that the decay becomes faster on decreasing χ. We recall that the decay of V_m as a function of τ is caused by the progressive smearing out of the spectral pattern of the population difference established by the preparative pulse (figure 1). So, the circumstance that this decay rate depends on χ suggests that the smearing rate depends on the particular distribution of $w(\Delta, \tau_1)$. This aspect will be discussed in the next section.

In a second set of experiments the interpulse distance τ and the Rabi frequency χ were kept fixed and we measured the echo amplitude V_m as a function of the first pulse duration τ_1. The echo amplitude decreases on increasing τ_1 because of the irreversible coherence loss mechanisms effective during both pulses for a total time span $2\tau_1$. We measured V_m as a function of τ_1 at various values of the Rabi frequency $\chi/2\pi$, ranging from 30 to 200 kHz. The experimental results are reported in figure 5 for three representative values of the Rabi frequency $\chi/2\pi$: 50, 100 and 200 kHz. As the time shape of $|M_\perp(t)|^2$ changes on varying τ_1, V_m was measured using the procedure described above and involving the extrema nearest to the echo centre. The results reported in figure 5 were taken using an interpulse distance $\tau = 150\ \mu$s; however, these decay curves did not change on varying τ, apart from obvious scale factors.

We note in figure 5 that, for each value of χ, the experimental data are well described by a single exponential decay, $[V_m \propto \exp(-\Gamma_E \tau_1)]$ with a power-dependent rate Γ_E. The values of Γ_E were determined by a best fit procedure and are reported in figure 6 as a function of the driving field intensity, both in frequency units. As shown, the power dependence of Γ_E is well described by a simple linear law $\Gamma_E = \alpha + \beta\chi$. By fitting we get $\alpha/2\pi = (2.0 \pm 0.4)$ kHz and $\beta = (2.6 \pm 0.4) \times 10^{-2}$. We note that the best fit value of $\alpha = (1.3 \pm 0.2) \times 10^4\ \mathrm{s}^{-1}$, i.e. the low-power limit of Γ_E, is compatible with the Bloch value $1/T_2$. The relationship between the power dependence of Γ_E ant that of the TN decay Γ_{TN} is examined in the next section.

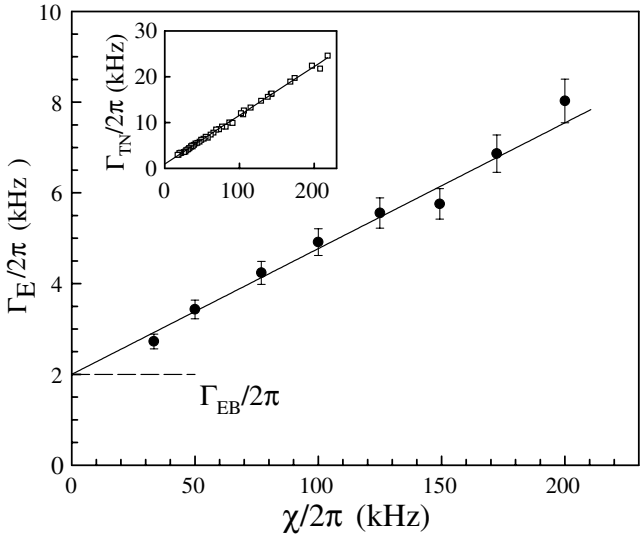

Figure 6. Dependence of the measured decay rate Γ_E on the Rabi frequency χ. The full line is the linear best fit to the experimental points. The intercept, (2.0 ± 0.4) kHz, is consistent with the value $\Gamma_{BE} = (T_2)^{-1}$ expected in the Bloch limit. The best fit slope is $\beta = (2.6 \pm 0.4) \times 10^{-2}$. The inset reports the experimental χ-dependence of the TN decay in the same sample (data taken from [9]).

4. Discussion

Firstly, we comment on the effect of varying the interpulse distance τ on the SNE amplitude. In our experimental conditions ($\tau \gg T_0$) the coherences induced during the preparative stage do not contribute to the SNE effect, which is caused mainly by the spectral pattern $w(\Delta, \tau_1)$ established at the end of the preparative pulse. According to the Bloch equations, this pattern tends to disappear during the interpulse distance because of longitudinal relaxation with the rate $T_1^{-1}(\approx 1\ \mathrm{s}^{-1}$ in our system). This prediction is in disagreement with our experimental results $V_m(\tau)$ (figure 4) in many respects: the decay is not a single exponential, the rate is much faster and it is also power dependent, as it decreases on increasing the power level, at least in the investigated range of χ. The SD may be the origin of so fast a decay. SD effects were not taken into account in the theoretical treatment outlined in section 2, where the spin packets were assumed to evolve in time, independently from each other. This approximation may be no longer valid in a timescale of the order of milliseconds. In fact the slow migration of the excitations over the whole resonance line may affect the persistence of the population spectral pattern stored during the first pulse. The SD process, usually faster than spin–lattice relaxation, may be the dominant cause of SNE decay at this timescale. In this regard we note that the excitation by the first pulse is spectrally selective in two aspects. On the one hand it involves only a narrow part of the resonance line (with a width of the order of χ, much less than the inhomogeneous width σ). This situation is usually described in terms of A-type (echo-active) spins and B-type (the others) spins [15, 40–42]. The dipolar interaction A–B drags spin excitations away from the line centre and contributes to the decay of the echo. On increasing χ, the number of A-type spins increases with respect to B-type spins; this circumstance may account for the slower decay of the echo at high χ, which has been experimentally observed. On the other hand, the first pulse excitation is spectrally selective also within the A-type spin group. In fact it establishes a comb pattern (figure 1) within the central part of the line, which is

the source of the SNE formation. So, one expects that the A–A dipolar interaction may smear this pattern and yield an additional contribution to the echo decay. The population pattern gets finer and finer on increasing τ_1, with higher spectral gradients of the population difference. So, this contribution to the decay rate is expected to increase on increasing τ_1. On the contrary, we observed that the experimental curves $V_m(\tau)$ are essentially independent of the value of τ_1. So, our experimental results suggest that the former effect (due to A–B interaction) is predominant.

Now, we discuss the role played by the irreversible decoherence mechanisms and their dependence on the field intensity. We recall that according to the Bloch equations the amplitude of the SNE is expected to decay on increasing τ_1 as a single exponential law $V_m \propto \exp(-\Gamma_{EB}\,\tau_1)$ with the rate $\Gamma_{EB} = 1/T_{2v}$. Contrary to this prediction, we found that the decay rate Γ_E is higher than the free decoherence rate and that it increases linearly with the field intensity, expressed as Rabi frequency (figure 6). We recall that, according to equation (10), the χ-dependence of Γ_E images the power dependence of the out-of-phase decoherence time T_{2v}. This anomalous (non-Bloch) χ-dependence of Γ_E is reminiscent of the non-Bloch decay of the TN regime, already observed in the same system under single pulse excitation [8, 9]. In those experiments, the decay rate Γ_{TN} of TN was found to tend to the Bloch value $(2T_2)^{-1}$ in the low-power limit and to increase linearly with χ. The experiments reported here show that the decay rate Γ_E of the SNE follows a qualitatively similar behaviour, confirming that both coherent regimes manifest the same field dependence of the irreversible coherence mechanisms, not accounted for by the Bloch model.

For the sake of comparison we report, in the inset of figure 6, the experimental χ-dependence of the Γ_{TN} as measured in the same sample and well fitted by the linear law $\Gamma_{TN} = \alpha' + \beta'\chi$ with $\alpha' \approx \alpha/2$ and $\beta' = (10.6 \pm 0.5) \times 10^{-2}$. This value of β' may be compared with the value of $\beta = (2.6 \pm 0.4) \times 10^{-2}$ inferred from SNE experiments. Even if the power dependence of decay rates is similar for the two regimes, the slopes are different, in the sense that the χ-sensitivity of Γ_E seems to be less than Γ_{TN}.

A qualitative explanation for this difference may be put forward by recalling the origin of the anomalous decay of the driven coherent regimes. The generic spin S_i of the system experiences a local dipolar field H_{Li} which is the superposition of the dipolar fields H_{ij} generated by all the neighbouring spins S_j. In the presence of an intense resonant field, the spins S_j undergo forced precessions, each at its own Rabi frequency $\beta_j = \sqrt{\chi^2 + \Delta_j^2}$ as caused by the inhomogeneous spreading of the detuning Δ. The local field $H_{Li}(t)$ at the site S_i is the superposition of many contributions $H_{ij}(t)$ each one modulated at a different frequency so that it appears noisy, with both in-phase and out-of-phase components. According to theory by Shakhmuratov *et al* [11], this modification of the dipolar field induced by the resonant radiation causes the linear dependence of the rate Γ_{TN} on χ. Obviously, the same mechanism is effective also during the second refocusing pulse. However, in TN experiments the field-modified dipolar interaction involves all the spins spectrally located in a narrow band of width χ around the excitation point. On the other hand, in SNE experiments this narrow band is strongly modulated by the comb pattern (figure 1) governed mainly by the first pulse duration τ_1. So, only a fraction of the spins are now involved in the echo formation and in the field modification of the dipolar interaction. This circumstance may lessen the χ-sensitivity of the decay rate Γ_E with respect to Γ_{TN}.

5. Conclusion

In conclusion, we have reported experimental results on the SNE in ESR systems. The timing and the shape of the echo pattern appear in agreement with the theory by Szabo and

Shakhmuratov [30, 31]. We have investigated the decay properties of the echo and found that the decay is strongly affected by the SD mechanism; our results are consistent with the prevalence of the A–B interaction over the A–A. Moreover, we studied the effect of the coherence loss (out-of-phase decoherence) during the exciting and the refocusing pulses. Our results evidence a non-Bloch behaviour similar to that observed in other coherent regimes, which we ascribe to the field-induced modification of the dipolar field. However, our results have evidenced that the coherence loss mechanisms effective in different coherent regimes feature a different sensitivity to the driving field intensity. We tentatively ascribed this difference to the different number of involved spins.

A final remark concerns the time distance between the maximum and the minimum nearest to the echo centre. As noted previously, the experimental value of this distance is somewhat longer than the theoretical one. Admittedly, we have not at the moment a satisfactory explanation of this disagreement. Even if this aspect seems to play no role in the decay properties considered in the present paper, it might be relevant by itself for a thorough understanding of the spin dynamics during the SNE generation. In this regard, the experimental study of the SNE echo excited by two pulses having different χ may yield additional information. Experimental and theoretical work is in progress in this direction.

Acknowledgments

Partial financial support has been given by the Italian Ministry for University and Scientific Research, by University of Palermo, Italy (International Cooperation Agreement Palermo-Kazan). Technical assistance by G Lapis is gratefully acknowledged. RNS acknowledges support from ISTC (2121), the Russian Foundation for Basic Research and the Fonds voor Wetenschappelijk Onderzoek Vlaanderen.

References

[1] DeVoe R G and Brewer R G 1983 *Phys. Rev. Lett.* **50** 1269
[2] Boscaino R, Gelardi F M and Messina G 1983 *Phys. Rev.* A **28** 495
[3] Szabo A and Muramoto T 1989 *Phys. Rev.* A **39** 3992
[4] Boscaino R and La Bella V M 1990 *Phys. Rev.* A **41** 5171
[5] Boscaino R and Gelardi F M 1992 *Phys. Rev.* A **45** 546
[6] Shakhmuratov R N and Szabo A 1993 *Phys. Rev.* B **48** 6903
[7] Szabo A and Kaarli R 1991 *Phys. Rev.* B **44** 12307
[8] Boscaino R, Gelardi F M and Korb J P 1993 *Phys. Rev.* B **48** 7077
[9] Agnello S, Boscaino R, Cannas M, Gelardi F M and Shakhmuratov R N 1999 *Phys. Rev.* A **59** 4087
[10] Shakhmuratov R N, Gelardi F M and Cannas M 1997 *Phys. Rev. Lett.* **79** 2963
[11] Shakhmuratov R N, Gelardi F M and Cannas M 1997 *SPIE Proc.* **3239** 206
[12] Shakhmuratov R N and Szabo A 1998 *Phys. Rev.* A **58** 3099
[13] Asadullina N Ya, Asadullin T Ya and Asadullin Ya Ya 2001 *J. Phys.: Condens. Matter* **13** 3475
[14] Asadullina N Ya, Asadullin T Ya and Asadullin Ya Ya 2001 *J. Phys.: Condens. Matter* **13** 5231
[15] Asadullina N Ya, Asadullin T Ya and Asadullin Ya Ya 2002 *J. Phys.: Condens. Matter* **14** 10349
[16] Hanamura E 1983 *J. Phys. Soc. Japan* **52** 3678
[17] Schenzle A, Mitsunaga M, DeVoe R G and Brewer R G 1984 *Phys. Rev.* A **30** 325
[18] Apanasevich P A, Kilin S Ya, Nizovtsev A P and Onishchenco N S 1986 *J. Opt. Soc. Am.* B **3** 587
[19] Wodkiewicz K and Eberly J H 1985 *Phys. Rev.* A **31** 2314
[20] Berman P R 1986 *J. Opt. Soc. Am.* B **3** 572
[21] Kessel A R, Shakhmuratov R N and Eskin L D 1988 *Zh. Eksp. Teor. Fiz.* **94** 202 (Engl. transl. 1988 *Sov. Phys.–JETP* **67** 2071)
[22] Burshtein A I and Malinovsky V S 1991 *J. Opt. Soc. Am.* B **8** 1098
[23] Malinovskii V S 1995 *Phys. Rev.* A **52** 4921
[24] Shakhmuratov R N and Szabo A 1993 *Laser Phys.* **3** 1042

[25] Alekseev A I and Basharov A M 1979 *Zh. Eksp. Teor. Fiz.* **77** 537 (Engl. transl. 1979 *Sov. Phys.–JETP* **50** 272)
[26] Kuz'min V S, Saiko A P and Fedoruk G G 1991 *Zh. Eksp. Teor. Fiz.* **99** 215 (Engl. transl. 1991 *Sov. Phys.–JETP* **72** 121)
[27] Furrer R, Fujara F, Lange C, Stehlik D, Vieth H M and Vollmann W 1980 *Chem. Phys. Lett.* **75** 332
[28] Ponte Goncalves A M and Gillies R 1983 *Chem. Phys. Lett.* **94** 21
[29] Fedoruk G G 1998 *J. Appl. Spectrosc.* **65** 420
[30] Szabo A and Shakhmuratov R N 1997 *Phys. Rev.* A **55** 1423
[31] Szabo A and Shakhmuratov R N 1998 *Izv. Ross. Akad. Nauk Ser. Fiz.* **62** 217 (Engl. transl. 1998 *Bull. Russ. Acad. Sci. Phys.* **62** 261)
[32] Ponti A and Schweiger A 1994 *Appl. Magn. Reson.* **7** 363
[33] Solomon I 1959 *Phys. Rev. Lett.* **2** 301
[34] Wong N C, Kano S S and Brewer R G 1980 *Phys. Rev.* A **21** 260
[35] Bai Y S, Yodh A G and Mossberg T W 1986 *Phys. Rev.* A **34** 1222
[36] Ardelean I, Kimmich R and Klemm A 2000 *J. Magn. Reson.* **146** 43
[37] Torrey H C 1949 *Phys. Rev.* **76** 1059
[38] Boscaino R and Messina G 1986 *Physica* C **138** 179
[39] Gromov I and Schweiger A 2000 *J. Magn. Reson.* **146** 110
[40] Boscaino R, Cannas M, Gelardi F M and Leone M 1996 *Nucl. Instrum. Methods Phys. Res.* B **116** 373
[41] Boscaino R, Gelardi F M and Cannas M 1996 *Phys. Rev.* B **53** 302
[42] Agnello S, Boscaino R, Cannas M and Gelardi F M 2001 *Phys. Rev.* B **64** 174423